Solid State Communications 223 (2015) 12–15

Contents lists available at ScienceDirect

Solid State Communications

journal homepage: www.elsevier.com/locate/ssc

Effects of inverse degree on electronic structure and electron energy-loss spectrum in zinc ferrites

D. Sun [a], M.X. Wang [a], Z.H. Zhang [a,*], H.L. Tao [a], M. He [a], B. Song [b], Q. Li [c]

[a] Liaoning Key Materials Laboratory for Railway, School of Materials Science and Engineering, Dalian Jiaotong University, Dalian 116028, China
[b] Academy of Fundamental and Interdisciplinary Sciences, Harbin Institute of Technology, Harbin 150080, China
[c] Department of Physics, The Chinese University of Hong Kong, Shatin, New Territories, Hong Kong

ARTICLE INFO

Article history:
Received 29 July 2015
Received in revised form
9 September 2015
Accepted 16 September 2015
Accepting editor: Dr. Xincheng Xie
Available online 25 September 2015

Keywords:
Zinc ferrite
Inverse structure
Electron energy-loss spectroscopy
First-principles calculation

ABSTRACT

First-principles calculations were performed to study the effects of inverse degree in zinc ferrite on electronic structure and properties. The electron energy-loss near-edge fine structure (ELNES) were simulated, and the splitting of peak and intensities of the oxygen K-edges can be used to identify the inversion of zinc ferrite. More Fe^{3+} transferring from the octahedral sites to the tetrahedral sites lead to the changing of the ligand shells surrounding the absorbing atom, accounting for the observed changing in ELNES. The standard criterion for determining the reversal extent of the cations in zinc ferrite by ELNES was given.

1. Introduction

Zinc ferrite, a well-characterized antiferromagnetic insulator, has attracted considerable attention due to its intriguing magnetic properties [1,2]. The spinel zinc ferrite has a general formula $ZnFe_2O_4$, where Zn ions and Fe ions are divalent and trivalent metal cations, respectively. The structure of $ZnFe_2O_4$ consists of a cubic close-packed array of oxygen ions, with metal cations distributed in one eighth of tetrahedral interstices (A sites) and half of the octahedral interstices (B sites) [3,4]. The $ZnFe_2O_4$ can be classified as normal or inverse structure, depending on the distribution of the metal ions over the tetrahedral and octahedral sites. In a normal spinel $(Zn)^{tet}[Fe]_2{}^{oct}O_4$, all of the occupied octahedral sites are Fe^{3+} ions. Whereas in a completely inverse spinel $(Fe)^{tet}[Zn,Fe]^{oct}O_4$, they are occupied by Zn^{2+} and Fe^{3+} ions with equal proportions. However, in an actual case, the spinel $ZnFe_2O_4$ is partially inversed and has cation distributions between these two extremes. The inversion parameter, δ ($0 \le \delta \le 1$), is defined as the fraction of the filled tetrahedral sites that are occupied by Fe^{3+} ions [5,6]. Using this parameter, the cation site occupation of $ZnFe_2O_4$ can be described with a general formula $(Zn_{1-\delta}Fe_\delta)^{tet}[Zn_\delta Fe_{2-\delta}]^{oct}O_4$, where the round and the square brackets represent the elements in A and B sites, respectively [7,8]. $ZnFe_2O_4$ with different inversion parameter can be synthesized experimentally with much nonequilibrium processing, including rapid quenching [9], changing the oxygen partial pressure [10], and adjusting the synthesis temperatures [3], etc. The change in atomic arrangement of Fe^{3+} ions and Zn^{2+} ions in zinc ferrites affect both its structural characteristics and physical properties that are sensitive to the crystalline structure, such as its lattice parameter, magnetic behavior, electronic structure, etc [10,11].

Consequently, scrutinizing the local atomic coordination environment of the $ZnFe_2O_4$ is extremely important in understanding its potentially applied properties. Many characterization techniques have been used to investigate the local atomic coordination environment of $ZnFe_2O_4$, including X-ray absorption fine structures [12], neutron diffraction [11,13], Mössbauer spectroscopy [14,15], and electron energy-loss spectrum (EELS) [3].

EELS attached to transmission electron microscopy (TEM) is a powerful analytical technique that can be utilized to obtain information on the structure, bonding and electronic properties of a material [16]. Especially, the electron energy-loss near-edge fine structure (ELNES) resolves electronic dipole transitions from the core states of a particular atom to unoccupied final states. ELNES is sensitive to variations of the chemical environment of a given element, reflecting directly the unoccupied states of the atoms. The experimental ELNES characterization for $ZnFe_2O_4$ has been performed to study the relation between the microstructure and magnetic properties [3]. Usually, information about the structure or bonding of the sample is determined from comparison between the acquired spectrum and the available reference spectrum. Unfortunately, there is no standard reference spectrum available

* Corresponding author. Tel.: +86 411 84105700; fax: +86 411 84109417.
E-mail address: zhzhang@djtu.edu.cn (Z.H. Zhang).

http://dx.doi.org/10.1016/j.ssc.2015.09.004
0038-1098/

for comparison in the literature. ELNES simulation based on the density functional theory (DFT) has become an established technique to predict and interpret EELS for materials [17]. It is needed to make a systematic study to clarify relationship between the electronic structure and the local atomic coordination with the help of the first principle calculations.

In this paper, we provide the theoretical ELNES data for the zinc ferrite with different cation distribution by the first-principle simulation. The changes in the splitting of peak and intensities of the oxygen K-edges can be used to identify the inversion degree of zinc ferrite. The determination on the reversal extent of the cations in experimented ELNES for zinc ferrite was realized.

2. Computational details

First-principles calculations based on density functional theory have been used for both geometry optimization and ELNES simulating with the CASTEP code [18]. The exchange-correlation energy is described by the Perdew–Burke–Ernzerhof (PBE) formalism of the generalized gradient approximation (GGA). Lorentz broadening function with a full width at maximum (FWHM) of 0.2 eV is used in the Brillouin zone spectral integration, and the spectra are further convolved with a Gaussian with a FWHM of 0.4 eV to take into account the spectral resolution. The valence electronic configurations for O, Zn, and Fe are O $2s^2 2p^4$, Zn $3d^{10}4s^2$, and Fe $3d^6 4s^2$, respectively. To ensure a good convergence of the DFT calculations, we carefully test the dependences of the total energy on the plane-wave cutoff energy and the k-point meshes. The wave functions were expanded in plane waves up to a cutoff energy of 500 eV, and a $2\times2\times2$ Monkhorst–Pack mesh as k-point sampling was used to sample the irreducible Brillouin zone. Geometry optimizations were performed to fully relax the atomic internal coordinates and the lattice parameters within the BFGS minimization algorithm. The self-convergence thresholds for maximum stress and maximum displacement between optimization cycles are 0.02 GPa and 5×10^{-4} Å. The structures were fully relaxed until the Hellmann–Feynman force was less than 0.01 eV/Å and the energy convergence was better than 5×10^{-6} eV/atom.

3. Results and discussions

The crystal structure of $ZnFe_2O_4$ used in our calculations are taken from the neutron powder data with the cubic space group *Fd3m* and the lattice parameters $a=b=c=8.412$ Å [19]. The configurations with different inversion degrees were studied in our work as shown in Fig. 1. Fig. 1(a) shows the ideal normal spinel structure of $ZnFe_2O_4$ with 56 atoms (the inversion parameter $\delta=0$); Fig. 1(b) shows the structure of $(Zn_6Fe_2)[Zn_2Fe_{14}]O_{32}$, in which two Zn atoms in tetrahedral sites and two Fe atoms in octahedral sites are inversed with each other ($\delta=0.25$); Fig. 1 (c) shows the structure of $(Zn_4Fe_4)[Zn_4Fe_{12}]O_{32}$, in which four Zn atoms in tetrahedral sites and four Fe atoms in octahedral sites are inversed ($\delta=0.5$); Fig. 1(d) shows the total inverse spinel structure $(Fe_8)[Zn_8Fe_8]O_{32}$ ($\delta=1$). The optimized lattice parameters and volumes for different inverse structures are shown in Table 1. The results show that the inversion between Zn and Fe does not deform the structure seriously after full relaxation, except a slight increase in the unit cell volume.

To get a further insight into the electronic structure and magnetic properties in zinc ferrite with different inverse degrees, the calculated total density of states (TDOS) and partial density of states (PDOS) for zinc ferrite with different inverse degrees are shown in Fig. 2. The TDOS of normal spinel $Zn_8Fe_{16}O_{32}$ is shown in Fig. 2(a), where the Fermi level is set at zero, and the system is an insulator, which is similar to previous calculations [10,20]. Fig. 2(b)–(d) shows the TDOS of zinc ferrite with different inversion parameters (i.e., $(Zn_6Fe_2)[Zn_2Fe_{14}]O_{32}$, $(Zn_4Fe_4)[Zn_4Fe_{12}]O_{32}$ and $(Fe_8)[Zn_8Fe_8]$

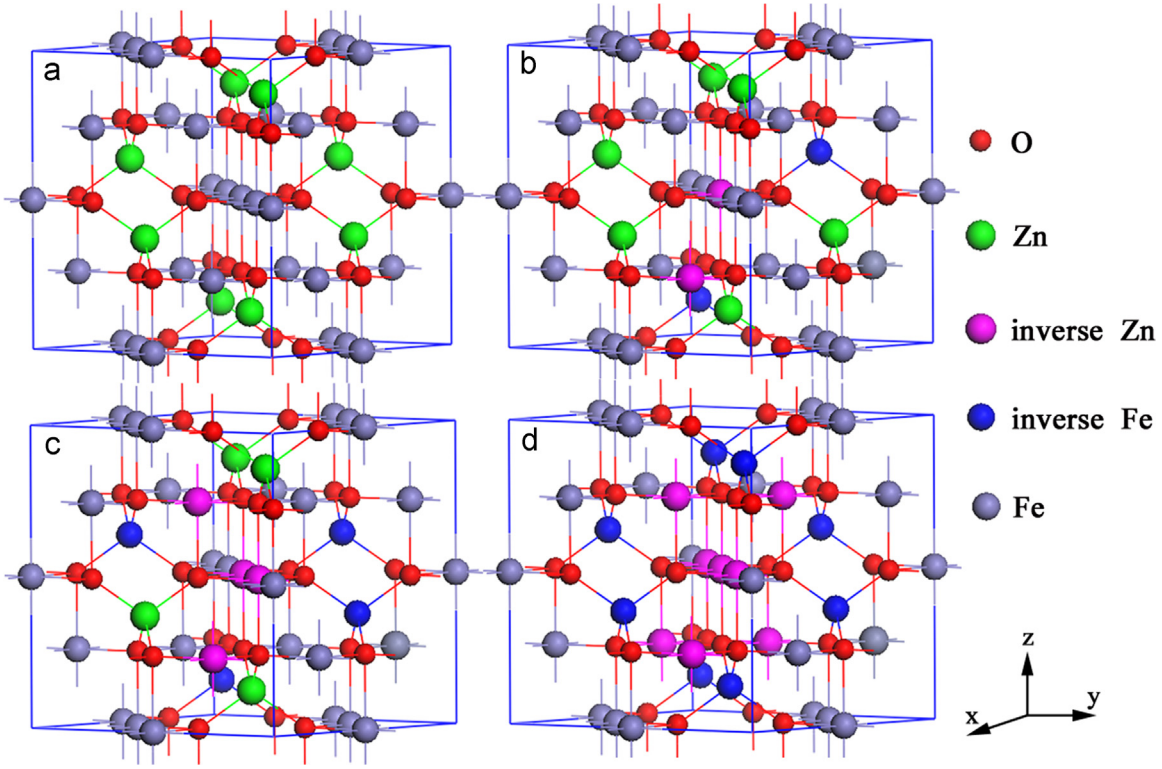

Fig. 1. (Color Online) Structural models for ELNES simulation: (a) $Zn_8Fe_{16}O_{32}$, (b) $(Zn_6Fe_2)[Zn_2Fe_{14}]O_{32}$, (c) $(Zn_4Fe_4)[Zn_4Fe_{12}]O_{32}$, (d) $(Fe_8)[Zn_8Fe_8]O_{32}$, respectively. The red, green, and purple spheres represent the oxygen, zinc, and iron atoms, respectively. The pink and blue atoms represent the inverted zinc and iron atoms, respectively.

O_{32}, respectively), where obvious changes of electronic structure are observed and the electronic bands near Fermi energy (E_F) become visibly narrower. Similarly, Fig. 2(e)–(h) shows the PDOS of zinc ferrite with different inversion parameters. Combined with the PDOS in Fig. 2(e)–(h), it is clearly recognizable that the TDOS between −8 eV and E_F is mainly governed by Fe-3d, Zn-3d, and O-2p orbital states. A careful analysis also demonstrates that the valence band mainly consists of Fe-3d and O-2p orbital states in the range of 1–2.5 eV. Compared with the result of $Zn_8Fe_{16}O_{32}$, the obvious spin imbalance (majority spin and minority spin is asymmetric) is appeared for the inversed structure, indicating the systems with high inversion degree have large magnetic moment. The results are consistent with the literatures [10,4]. The magnetic moment in zinc ferrite with different inverse degrees mainly comes from O-2p orbital and Fe-3d orbital, and the Zn atoms make a small contribution to the net magnetic moment from the partial density of states (PDOS) in Fig. 2(e)–(h). This is because that the magnetic moment mainly originates from the A–O–B superexchange interactions [21]. The cation inversion in zinc ferrite leads to the A–O–A and A–O–B superexchange interactions between the Fe^{3+} cations. The strength of the superexchange interaction depends on the angle and distances between metal–O–metal. In zinc ferrite, A–O–B superexchange is the strongest and A–O–A superexchange is the weakest. Such interaction does not exist in normal spinel zinc ferrite, because all Fe^{3+} are located in B sites, results in B–O–B antiferromagnetic coupling [22,23].

Table 1
Calculated lattice parameters (*a*, *b*, and *c*) and unit cell volume (*V*) after the optimization for the different inverse structures.

Configurations	Cell constant (Å)			Volume ($Å^3$)
	a	*b*	*c*	
$Zn_8Fe_{16}O_{32}$	8.187	8.187	8.187	548.75
$(Zn_6Fe_2)[Zn_2Fe_{14}]O_{32}$	8.173	8.222	8.173	549.21
$(Zn_4Fe_4)[Zn_4Fe_{12}]O_{32}$	8.247	8.131	8.201	549.93
$(Fe_8)[Zn_8Fe_8]O_{32}$	8.182	8.181	8.247	551.03

The effect of inversion between Zn and Fe of zinc ferrite was further studied by EELS simulations. When an electron is excited from a low-lying core state to a conduction band, a 'core hole' was leaved in place. Thus the core hole effect [24] was involved in our EELS modeling to get a better results. The theoretical ELNES spectra of O K-edges with different inverse degrees are shown in Fig. 3(a)–(d). In order to facilitate the analysis of spectral structures, all theoretical spectra have been aligned using the edge onset of the 10 eV. In the spectra of the O K-edge four main feature groups were observed, labeled as groups of peak A, peak B, peak C, and peak D [25]. According to the DOS calculations in Fig. 2, peaks A and B in the region 10–23 eV originate from electron transitions from O 1*s* to the unoccupied states in the O 2*p* orbitals hybridized with Fe 3*d* orbitals, and to higher-energy orbitals consisted mainly of 4*sp* levels of Zn and Fe, respectively. Peak C and D come from the electron backscattering of the nearest and second nearest coordination shells around ionized O atoms, respectively [25]. However, for configurations with different inversion parameters, different shapes and intensities are observed, especially one can see a subtle difference in the split of peak A (labeled as a_1 and a_2). The relative intensity a_1/a_2 become larger and the separation between a_1 and a_2 changes a little with the increasing of the inverse degree. In the oxygen K-edge spectra, the splitting of the feature A into two components has been interpreted with respect to t_{2g} and e_g symmetry bands separated by the ligand-field splitting to a first approximation [26]. With the increasing of the inversion degree, the local structural changes involving considerable Fe cations transference from B to A sites. The number of Fe^{3+} in A sites become larger and larger, correspondingly, the particular configuration of the ligand shells surrounding the absorbing atom

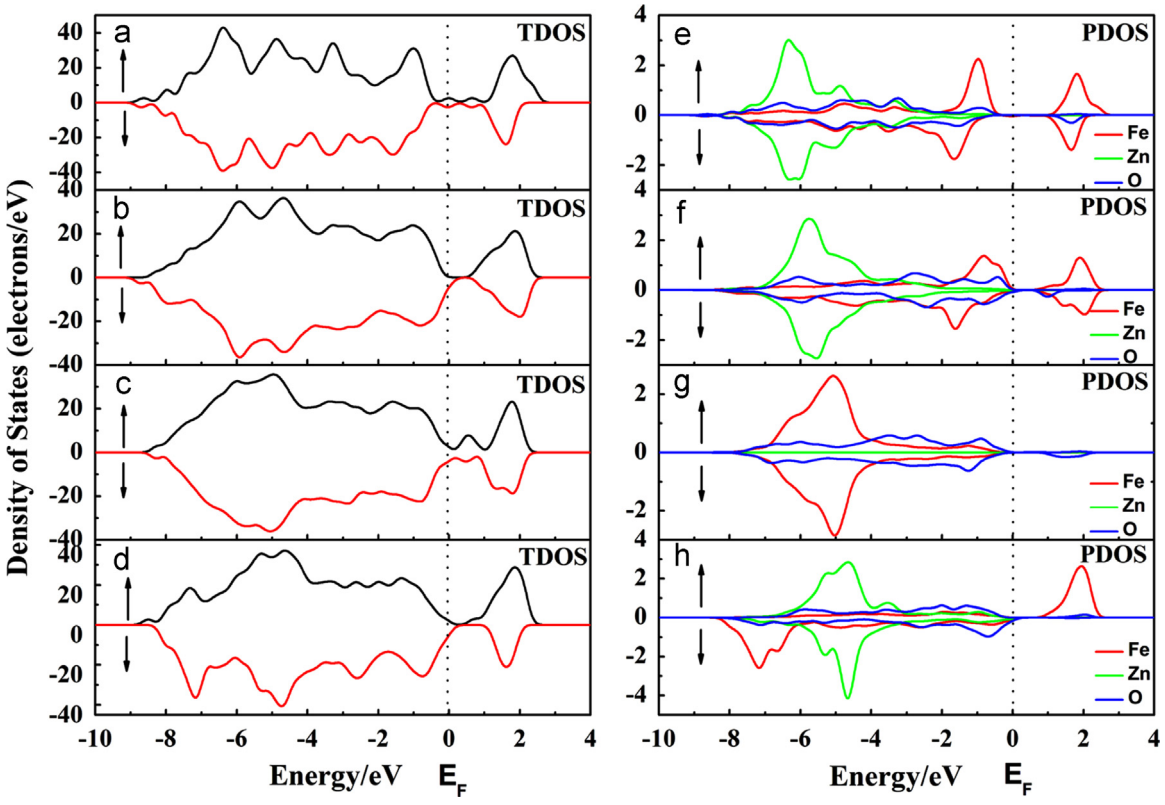

Fig. 2. (Color Online) TDOS for (a) $Zn_8Fe_{16}O_{32}$, (b) $(Zn_6Fe_2)[Zn_2Fe_{14}]O_{32}$, (c) $(Zn_4Fe_4)[Zn_4Fe_{12}]O_{32}$, and (d) $(Fe_8)[Zn_8Fe_8]O_{32}$, respectively. PDOS for (e) $Zn_8Fe_{16}O_{32}$, (f) $(Zn_6Fe_2)[Zn_2Fe_{14}]O_{32}$, (g) $(Zn_4Fe_4)[Zn_4Fe_{12}]O_{32}$, and (h) $(Fe_8)[Zn_8Fe_8]O_{32}$, respectively.

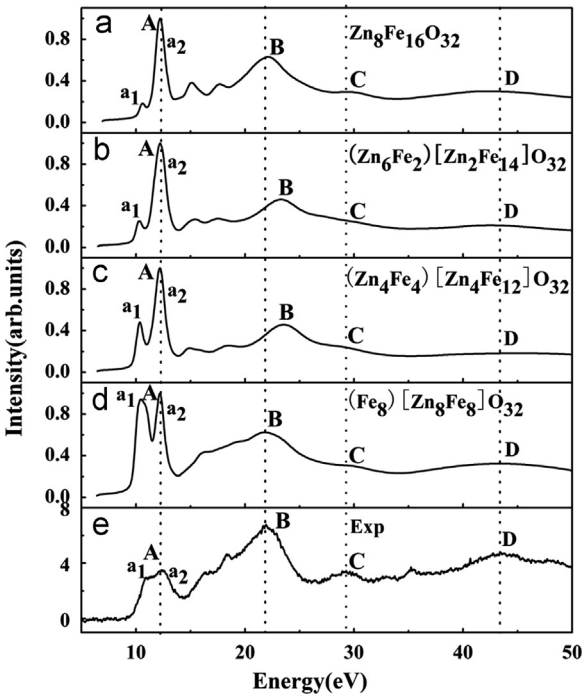

Fig. 3. The calculated ELNES of O K-edge for zinc ferrite with different inverse degrees, (a) $Zn_8Fe_{16}O_{32}$, (b) $(Zn_6Fe_2)[Zn_2Fe_{14}]O_{32}$, (c) $(Zn_4Fe_4)[Zn_4Fe_{12}]O_{32}$, (d) $(Fe_8)[Zn_8Fe_8]O_{32}$, and (e) the experimental spectra cited from reference [3] for comparison.

(oxygen atom) was changed. From Fig. 2, more O-2p, Fe-3d hybridization state appeared in the unoccupied states, thus the a_1/a_2 ratio increases with the increasing of the inverse degree. For comparison, the experimental spectrum from the Literature [3] is shown in Fig. 3(e). The dominant features of O-K edge experimental spectrum are very similar to Fig. 3(d) in our work, indicating the configuration is nearly to the total inverse spinel structure. Thus the spectra shown in Fig. 3 can be seen as the standard criterion for determining the reversal extent of the cations in zinc ferrite.

4. Conclusions

In summary, the electronic structure and ELNES data of $ZnFe_2O_4$ with different inverse degrees were calculated by the first-principles calculations. Compared with the normal spinel $ZnFe_2O_4$, obvious changes of electronic structure are observed with the increasing of the inverse degree and the magnetic moment were observed. Different shapes and intensities are observed in O-K edge, which is related to the Fe^{3+} around the oxygen atoms and the a_1/a_2 ratios become larger with the increasing of the inversion degree. The reversal extent of the cations in zinc ferrite can be determined by the standard criterion in this work.

Acknowledgment

This work was sponsored by National Natural Science Foundation of China under Grant nos. 51372027, 51372026, and No.51372056

References

[1] R. Rameshbabu, R. Ramesh, S. Kanagesan, A. Karthigeyan, S. Ponnusamy, J. Supercond. Nov. Magn. 27 (2014) 1499–1502.
[2] C. Yao, Q. Zeng, G. Goya, T. Torres, J. Liu, H. Wu, M. Ge, Y. Zeng, Y. Wang, J. Jiang, J. Phys. Chem. C. 111 (2007) 12274–12278.
[3] X. Guo, H. Zhu, M. Si, C. Jiang, D. Xue, Z. Zhang, Q. Li, J. Phys. Chem. C. 118 (2014) 30145–30152.
[4] S. Nakashima, K. Fujita, K. Tanaka, K. Hirao, T. Yamamoto, I. Tanaka, Phys. Rev. B 75 (2007) 174443.
[5] H. Ehrhardt, S. Campbell, M. Hofmann, J. Alloy. Compd. 339 (2002) 255–260.
[6] J. Wu, N. Li, J. Xu, Y. Jiang, Z.-G. Ye, Z. Xie, L. Zheng, Appl. Phys. Lett. 99 (2011) 202505.
[7] F. Docherty, A. Craven, D. McComb, J. Skakle, Ultramicroscopy 86 (2001) 273–288.
[8] S.N. Rishikeshi, S.S. Joshi, M.K. Temgire, J.R. Bellare, Dalton Trans. 42 (2013) 5430–5438.
[9] Katsuhisa Tanaka, Yoh Nakahara, Kazuyuki Hirao, Naohiro Soga, J. Magn. Magn. Mater. 131 (1994) 120–128.
[10] C. Jin, P. Li, W. Mi, H. Bai, J. Appl. Phys. 115 (2014) 213908.
[11] M. Hofmann, S. Campbell, H. Ehrhardt, R. Feyerherm, J. Mater. Sci. 39 (2004) 5057–5065.
[12] C. Upadhyay, H. Verma, V. Sathe, A. Pimpale, J. Magn. Magn. Mater. 312 (2007) 271–279.
[13] H. Ehrhardt, S. Campbell, M. Hofmann, Scr. Mater. 48 (2003) 1141–1146.
[14] H.H. Hamdeh, J. Ho, S. Oliver, R. Willey, G. Oliveri, J. Appl. Phys. 81 (1997) 1851–1857.
[15] S. Ayyappan, S.P. Raja, C. Venkateswaran, J. Philip, B. Raj, Appl. Phys. Lett. 96 (2010) 143106.
[16] J. Lu, S.-P. Gao, J. Yuan, Ultramicroscopy 112 (2012) 61–68.
[17] S.J. Clark, M.D. Segall, C.J. Pickard, P.J. Hasnip, M.I. Probert, K. Refson, M.C. Payne, Z. Krist. 220 (2005) 567–570.
[18] F. Lopez, A. López-Delgado, J.M. de Vidales, E. Vila, J. Alloy. Compd. 265 (1998) 291–296.
[19] C. Cheng, C.-S. Liu, J. Phys.: Conf. Ser. 145 (2009) 012–028.
[20] F. Li, L. Wang, J. Wang, Q. Zhou, X. Zhou, H. Kunkel, G. Williams, J. Magn. Magn. Mater. 268 (2004) 332–339.
[21] R. Rameshbabu, R. Ramesh, S. Kanagesan, A. Karthigeyan, S. Ponnusamy, J. Mater. Sci. Mater. Electron. 25 (2014) 2583–2588.
[22] E.J. Choi, Y. Ahn, E.J. Hahn, J. Korean Phys. Soc. 53 (2008) 2090–2094.
[23] S.-P. Gao, C.J. Pickard, M.C. Payne, J. Zhu, J. Yuan, Phys. Rev. B 77 (2008) 115122.
[24] C. Colliex, T. Manoubi, C. Ortiz, Phys. Rev. B 44 (1991) 11402.
[25] F. De Groot, M. Grioni, J. Fuggle, J. Ghijsen, G. Sawatzky, H. Petersen, Phys. Rev. B 40 (1989) 5715.
[26] S. Stewart, S. Figueroa, J.R. López, S. Marchetti, J. Bengoa, R. Prado, F. Requejo, Phys. Rev. B 75 (2007) 073408.